

The Unusual Temporal and Spectral Evolution of SN2011ht. II. Peculiar Type II_n or Impostor? ¹

Roberta M. Humphreys,² Kris Davidson,² Terry J. Jones,² R. W. Pogge,³ Skyler H. Grammer,² José L. Prieto,⁴ T. A. Pritchard,⁵

ABSTRACT

SN2011ht has been described both as a true supernova and as an impostor. In this paper, we conclude that it does not match some basic expectations for a core-collapse event. We discuss SN2011ht's spectral evolution from a hot dense wind to a cool dense wind, followed by the post-plateau appearance of a faster low density wind during a rapid decline in luminosity. We identify a slow dense wind expanding at only 500–600 km s⁻¹, present throughout the eruption. A faster wind speed $V \sim 900$ km s⁻¹ occurred in a second phase of the outburst. There is no direct or significant evidence for any flow speed above 1000 km s⁻¹; the broad asymmetric wings of Balmer emission lines in the hot wind phase were

¹Based on observations with the Large Binocular Telescope (LBT), an international collaboration among institutions in the United States, Italy and Germany. LBT Corporation partners are: The University of Arizona on behalf of the Arizona university system; Istituto Nazionale di Astrofisica, Italy; LBT Beteiligungsgesellschaft, Germany, representing the Max-Planck Society, the Astrophysical Institute Potsdam, and Heidelberg University; The Ohio State University, and The Research Corporation, on behalf of The University of Notre Dame, University of Minnesota and University of Virginia. Based also on observations obtained at the MMT Observatory, a joint facility of the Smithsonian Institution and the University of Arizona, on data from the NASA/ESA *Hubble Space Telescope* obtained at the Space Telescope Science Institute, operated by the Association of Universities for Research in Astronomy, Inc., under NASA contract NAS5-26555, and on observations from the Gemini Observatory, operated by the Association of Universities for Research in Astronomy, Inc., under a cooperative agreement with the NSF on behalf of the Gemini partnership: the National Science Foundation (United States), the Science and Technology Facilities Council (United Kingdom), the National Research Council (Canada), CONICYT (Chile), the Australian Research Council (Australia), Ministério da Ciência e Tecnologia (Brazil) and Ministerio de Ciencia, Tecnología e Innovación Productiva (Argentina).

²Minnesota Institute for Astrophysics, 116 Church St SE, University of Minnesota, Minneapolis, MN 55455; roberta@umn.edu, kd@astro.umn.edu

³Department of Astronomy, The Ohio State University, 140 W. 18th Ave., Columbus, Ohio 43210

⁴Department of Astrophysical Sciences, Princeton University, Princeton, NJ 08544

⁵Department of Astronomy & Astrophysics, Penn State University, 525 Davey Lab, University Park, PA 16802

due to Thomson scattering, not bulk motion. We estimate a mass loss rate of order $0.05 M_{\odot} \text{ y}^{-1}$ during the hot dense wind phase of the event. The same calculations present difficulties for a hypothetical unseen SN blast wave. There is no evidence that the kinetic energy greatly exceeded the luminous energy, roughly 3×10^{49} ergs; so the radiative plus kinetic energy was small compared to a typical SN. *We suggest that SN2011ht may have been a giant eruption driven by super-Eddington radiation pressure, perhaps beginning a few months before the discovery. A strongly non-spherical SN might also account for the data, at the cost of more free parameters.*

Subject headings: supernovae: individual:(SN2011ht)

1. Introduction

Our multi-wavelength observations of SN2011ht have revealed an unusual eruption which shares characteristics with both the Type IIn supernovae and the SN impostors, Paper I (Romig et al 2012). The first spectrum of SB2011ht obtained shortly after discovery (Pastorello et al. 2011) resembled the dense winds observed in some Luminous Blue Variables (LBVs) at maximum, the Intermediate-Luminosity Red Transients (ILRTs) such as SN2008S and NGC 300-OT2008 (Smith et al. 2009, Bond et al. 2009, Berger et al. 2009, Humphreys et al. 2011) and the warm hypergiant IRC+10420. With a luminosity of $M_v \sim -14$ mag at its discovery, SN2011ht was designated an “impostor” (CBET 2851, PSN J10081059+5150570). Shortly afterward, however, it brightened about two magnitudes in the visual, reaching $M_v \sim -17$ mag, at its distance of 19.2 Mpc in UGC 5460 (Romig et al 2011). Based on its luminosity and narrow hydrogen emission lines, Prieto et al. (2011a,b) suggested that it was a true supernova of Type IIn. Simultaneous with its visual brightening, SN2011ht also showed a rise in its UV flux, increasing 7 magnitudes in 40 days (Romig et al. 2011). SN2011ht is one of only a few Type IIn SNe observed in the near-UV and has the most complete observations showing its rise to the UV and visual maxima.

The first spectra obtained by our group after the rise in UV flux were dominated by strong Balmer emission with P Cygni absorption and very broad asymmetric wings characteristic of Thomson scattering plus peculiar broad He I emission. It resembled a dense, hot stellar wind (see Fig. 3 in Paper I). In Paper I we attributed this peculiar spectrum to the interaction of the shock with the ejection of a shell of material a year before the explosion. However, the last spectrum published in Paper I showed the onset of a major spectroscopic change with the appearance of absorption and emission lines characteristic of a much cooler wind as the luminosity began to decrease. A later spectrum from mid January revealed a

fully developed dense wind resembling a late F-type or early G-type supergiant with strong absorption lines, plus H, the Ca II triplet and Fe II in emission with deep P Cygni profiles (Humphreys 2012). Shortly after that, SN2011ht began a rapid decline in the visual. A spectrum obtained shortly after the decline began shows another dramatic change; to a thin, warm wind characteristic of high mass losing luminous stars and some giant eruption LBVs. In many ways, SN2011ht closely resembles SN1994W (Chugai et al 2004, Dessart et al. 2009), SN1998S (Chugai 2001), and SN2009kn a twin of SN1994W (Kankare et al. 2012). In this paper we emphasize that SN2011ht’s development seems consistent with a radiation-driven eruption not a conventional hypersonic blast wave. The characteristic speeds are less than 1000 km s^{-1} .

The new observations including near UV spectra from HST/STIS/MAMA and near and mid-infrared photometry are described in the next section. The evolution of its spectrum and the kinematics of the ejecta are discussed in sections 3 and 4. In section 5 we demonstrate that the asymmetric wings are consistent with Thomson scattering and use a scattering model to estimate the mass loss rate. The post-decline spectral energy distribution and dust formation properties are discussed in section 6. The changing character and physical properties in the ejecta as the eruption progressed are reviewed in section 7. In the last section we show that there is no observational evidence that SN2011ht was a terminal explosion and propose an alternative explanation for its eruption.

2. Multi-wavelength Observations and Data Reduction

Our observations of SN2011ht range from the near ultraviolet beginning shortly after its discovery to the near and mid-infrared at later times.

2.1. Ultraviolet, Optical and Near and Mid-Infrared Imaging and Photometry

The *Swift* UVOT photometric measurements are described in Paper I with a table of observations beginning only 5.8 days after discovery from JD 5838.6 to JD 5950.7, shortly before it began its rapid visual decline. The subsequent *Swift* measurements are in Table 1, and in Figure 1 we show the complete multi-wavelength light curve from *Swift*. Unfortunately no observations were obtained by our group during the initial decline.

The rapid decline by about 4.5 magnitudes in only 25 days was suggestive of dust formation. We therefore obtained JHK_s photometry with the Lucifer near-infrared imager on the Large Binocular Telescope (LBT) on 13 March 2012 (JD5999.6). The seeing was 0.9,

FWHM. A star in the field, 2MASS 10081759+5151289, with magnitudes $J = 10.83$, $H = 10.40$, and $K_s = 10.24$, was used for the flux calibration. This star was slightly saturated in the images, complicating our data reduction. The flux was estimated by fitting the 2MASS star’s image profile with a measured, scaled profile from a nearby fainter source for pixels greater than $0''.6$ (5 pixels) from the image center. The flux was then computed using the area under this scaled profile. Our internal errors were 0.02 mag or less at H and Ks, but due to uncertainties in our computation of the comparison star’s flux, we have included an additional error of 0.1 mag in Table 2.

Visual ugr photometry was measured shortly afterwards on 25 March 2012 with the MODS imager on the LBT with a $6' \times 6'$ FOV and spatial scales of $0.240''/\text{pixel}$ and $0.246''/\text{pixel}$ in the blue and red, respectively. The magnitudes were measured differentially with respect to seven isolated stars on the frame from the SDSS DR6 using aperture photometry with the QPHOT routine in IRAF. The errors were determined by normal error propagation including the photometric errors of the reference stars. The resulting spectral energy distribution (Figure 2) showed that SN2011ht was very red after the rapid decline, with a rise in flux in the near-infrared, a probable signature of dust emission at longer wavelengths.

We therefore requested and were granted Director’s Discretionary Time on Gemini-N for mid-infrared observations at L' and M' with NIRI. Due to scheduling constraints and instrument availability the observations were not obtained until 03 May 2012. Images were acquired at 2.2, 3.8 and $4.7\mu\text{m}$. HD 84800 was used as a standard star with assumed magnitudes of $K = 7.54$, $L' = 7.55$, and $M' = 7.56$. Seeing was consistently under $0''.4$. A synthetic aperture of $0''.86$ was used for the standard and SN2011ht. For the L' and M' filters, images were taken in a 9 dither pattern, spaced $3''$ apart in RA and DEC. Sky background images were formed from the 8 other dither positions and subtracted from each dither position. These 9 images were then shifted and stacked to produce the final image. The 3σ upper limit for the $4.7\mu\text{m}$ photometry was determined from the rms fluctuations in the final image and the size of the synthetic aperture.

The resulting visual and infrared magnitudes are summarized in Table 2 and the SED is shown in Figure 2. Although delayed, the L' and M' measurements confirm the formation of dust. The spectral energy distribution and dust formation are discussed in §6.

2.2. Spectroscopy

Spectra were observed with several different telescopes beginning shortly after SN2011ht’s discovery until it became too faint during the rapid decline. The observations described in Paper I include spectroscopy with the Hobby-Eberly Telescope (HET) LRS, the *Swift* UVOT uv grism, the Astrophysical Research Corporation (ARC) telescope DIS, and the Large Binocular Telescope (LBT) MODS1. The details are described in Paper I. Additional groundbased spectra discussed in this paper were observed with the MMT Hectospec MOS on 23 January and 13 February 2012. The Hectospec spectra were obtained with the low resolution 270l grating yielding a wide wavelength coverage from 3650 – 9200Å with a FWHM resolution of 5Å. The spectra were bias subtracted, flat-fielded and wavelength calibrated in the Hectospec pipeline at the Center for Astrophysics and flux calibrated.

As discussed in Paper I, SN2011ht is distinguished by its rapid rise in the ultraviolet, strong UV flux, and a steeply rising flux in its near-UV spectra. For these reasons we requested and were granted Director’s Discretionary Time with the *Hubble Space Telescope* for near UV spectroscopy with STIS/MAMA. Spectra were observed in three wavelength regions, NUV2800, NUV2376, and FUV1425 on 26 December 2011, and were processed through the calstis pipeline at STScI. Unfortunately these observations occurred just a few weeks too late to see the UV-bright phase. Details of the observations are included in Table 3 together with the other spectra discussed in this paper.

3. Evolution of the Spectrum

The spectrum of SN2011ht has shown some remarkable and fairly rapid changes from its initial “dense wind” at discovery, to the hot dense wind spectrum described in Paper I, and the transition to the cool dense wind observed later. Our spectra showing the transition from the hot dense wind to the cool dense wind are shown in Figure 3. Line identifications and the measured Doppler velocities with their 1σ errors are summarized in Tables 4 and 5 at four significant times; the dense hot wind, the transition, the cool dense wind and a warm lower density wind during the decline. The spectra at these four times are discussed separately in the subsections below.

3.1. The Hot Dense Wind Spectrum

The spectra obtained by our group immediately after the rise in the UV flux are shown in Paper 1. The spectra from that period correspond to the maximum in the UV flux. Our

spectra observed between 01 and 23 November 2011 show strong narrow Balmer emission lines with P Cygni absorption profiles and very broad emission wings. The wings are asymmetric to the red, a classic signature of Thomson scattering (Figure 8). The emission wings on the Balmer lines extend from ~ -4700 to $+8000$ km s $^{-1}$ in H α , but, as discussed in §5 the broad wings are due to scattering by the electrons not bulk motion. The two strong He I emission lines at $\lambda 5876\text{\AA}$ and $\lambda 7065\text{\AA}$ are especially peculiar with very broad asymmetric wings extending from -2600 to 5500 km s $^{-1}$ while the other He I lines show only weak emission and P Cygni absorption profiles similar to the hydrogen lines. Overall, the spectrum suggests a hot, dense wind, and in Paper I, Figure 9, a maximum temperature of $\sim 13,000$ K was estimated for the wind. However the strong UV flux and the very steep rise in the near UV flux in the MODS1 spectrum are not characteristic of a dense wind. The MODS1 spectrum from 17 November 2012 is shown here in Figure 4. Although the emission lines and the absorption features were listed in Paper I with their blueshifted velocities relative to the galaxy, due to a small zero point error in the wavelengths, they are repeated here in Table 4 with their measured Doppler velocities.

The P Cygni absorption components in the stronger Balmer lines are blueshifted relative to the emission by about 550 km s $^{-1}$ supporting an expansion of the ejecta by approximately this amount. We avoid using the FWHM of the Balmer emission lines to measure the velocity of the ejecta or wind because the line profiles are distorted on the red side by the strong scattering wings. The absorption components are likewise altered by the strong emission. Therefore, as the emission weakens in the higher Balmer lines, the velocities of the Balmer absorption lines increase. The spectrum also shows strong absorption from the O I triplet at $\lambda 7774\text{\AA}$, a high luminosity indicator in A to F-type supergiants, plus a weak Ca II K line. The O I and K-line velocities are comparable to those of the higher Balmer absorption lines, not affected by emission lines, indicating that these lines are formed in the expanding ejecta. Although these lines are usually identified with somewhat lower temperatures, the O I triplet and a weak K line are observed in luminous supergiants with temperatures $\leq 15,000$ K

Another peculiarity is the presence of three very broad absorption features in the near-UV in the MODS1 spectra. These absorption features are unidentified, and are clearly present in both MODS1 spectra from November. They are not the atmospheric O $_3$ Huggins bands which are bluer and narrower and can be identified in the same spectra. They are not instrumental because they are not seen in the standard star spectra, and are too sharp to be artifacts of the response. They also do not correspond to any night-sky emission lines. Given their appearance, regular spacing, and sharp red edges, they are probably

molecular. The wavelengths of the red edges are $\lambda\lambda 3396$, 3528 , and 3659\AA ¹. We conclude that these absorption bands are real and are most likely formed near SN2011ht and probably in the ejecta. They could be diffuse interstellar bands (DIBs), but none are known at these wavelengths.

3.2. The Transition

The last spectrum described in Paper I from 21 Dec. 2011 (see Figure 3) shows the onset of the transition from the hot wind to the cool dense wind as the total luminosity and the near-UV flux declined during this time. The MODS1 spectra from 26 and 28 December 2011 (Figure 5) show a well developed spectrum of Fe II absorption and emission lines, Ca II H and K absorption, and the appearance of the near-infrared Ca II triplet in absorption. The Balmer lines still show the strong asymmetric emission profiles with P Cygni absorption. The He I emission is gone, but an excess of flux is still present in the near-UV plus a strong forest of Fe II absorption lines.

We have four spectra from this period obtained only a few days apart that illustrate the relatively rapid transition. There are no apparent P Cygni absorption components in the Balmer lines in the HET 21 December spectrum, although they are clearly visible in the MODS1 spectrum a few days later. This difference is due to the lower resolution in the HET spectrum. In this series of spectra, the Fe II absorption lines increase in strength with time, the O I $\lambda 7774$ and $\lambda 8446$ absorption lines increase, and the Ca II triplet appears. Between 21 December to 02 January the equivalent widths of the Ca II lines nearly doubled. Similarly, the O I triplet and the Fe II absorption lines in the blue increased by about a factor of 1.5 in equivalent width.

3.3. The STIS/MAMA Ultraviolet Spectra

As we noted earlier, SN2011ht’s UV flux and steep continuum in the near-ultraviolet in the MODS1 spectrum from 17 November 2011 are not characteristic of a dense wind, even a very hot one. The strong UV flux might be due to shock breakout from the dense circumstellar medium as suggested for PTF09UJ (Ofek et al. 2010), although we would expect the UV peak to be brief and the temperature to drop not rise after the breakout.

¹Correcting for the redshift of UGC 5460 of 1093 km s^{-1} , the corresponding wavelengths are 3384 , 3515 , and 3546\AA

Consequently, these features raise questions about how the object can produce such a steep near-UV continuum if the wind is opaque and if it isn't opaque, how does it produce a continuum with a supernova-like brightness plus emission lines with such strong Thomson scattering (see §5 below). To answer these questions we obtained near-UV spectra shortward of 3300Å with STIS/MAMA for independent information on its temperature and other parameters. Unfortunately, the spectra were obtained just after the UV flux had begun to decline and when the groundbased spectra showed the appearance of the absorption and emission lines of Fe II signalling a decrease in temperature of the wind.

The MAMA spectra were observed on the same date as the MODS1 spectrum from 26 December 2011. The NUV2376 spectrum and MODS1 blue spectrum almost overlap and are shown together in Figure 5. Both spectra show a forest of absorption lines (Fe II, Cr II, Mn II) shortwards of the Balmer jump common in the spectra of supergiants with temperatures below about 12,000K. Other strong features in the near UV spectra include the Mg II doublet at $\lambda 2800\text{\AA}$ in absorption. The absorption lines of Si II, Si III, and N III reported in the earlier *Swift* uv spectra (Paper I) are not present.

3.4. The Cool Dense Wind

Figure 6 shows the Hectospec spectrum for 23 January 2012 together with the MODS1 26 December spectra for comparison. The 23 January spectrum shows the fully developed cool, dense wind. Although SN2011ht was still visually bright it was fading in *b* and *u*. The absorption line spectrum resembles that of an early G-type star with a strong G band plus high luminosity features such as the blends near $\lambda 4172\text{\AA}$ and $\lambda 4177\text{\AA}$. The Balmer lines are still in emission with broad asymmetric wings but with noticeably weaker emission, and the P Cygni absorptions are much deeper relative to the continuum. The Ca II triplet absorption lines have continued to increase in strength and now show strong P Cygni profiles with broad emission wings asymmetric to the red like the Balmer lines. The Ca II triplet emission lines are formed in the star's ejecta by radiative de-excitation from the strong Ca II H and K absorption upper levels. Ca II has a low ionization potential and is suppressed in the presence of UV radiation consequently, the emission only began to weakly appear in the transition spectra with the decline of the UV flux. The Fe II absorption lines are also stronger and their corresponding emission features when present are much weaker. We also note a strong Na I D line with a P Cygni profile.

3.5. The Decline – a Low Density Wind

We have three spectra observed in February 2012 during SN2011ht’s rapid decline in apparent brightness. The spectra from 13 February and 28 February, 2012 are shown in Figure 7. Although, all three exposures are weak with low S/N, they are essentially identical. The strong absorption line spectrum is gone. The spectra show $H\alpha$, $H\beta$, $H\gamma$, the Ca II triplet, and weak [Ca II] $\lambda\lambda 7291$ and 7323 in emission. Four Fe II emission lines are also identified. The Na I D doublet still has a P Cygni-type profile. Although the Ca II triplet no longer shows absorption components, the emission lines are still noticeably asymmetric to the red. The scattering wings on the Balmer lines however are gone, but $H\alpha$ and $H\beta$ still have weak P Cygni-type absorption. The only absorption lines, not altered by emission, are $H\delta$ and He and they have velocities consistent with the absorption lines measured at the earlier times. The presence of the rare [Ca II] emission doublet indicates a very low density optically thin region. The transition that produces the triplet emission leaves the ions in the upper level for the [Ca II] forbidden lines. These ions are normally collisionally de-excited back to the ground state that produces the H and K lines, unless the density is sufficiently low.

Our spectrum from 13 February was observed when the object was about 18th magnitude (Figure 1) and had decreased by 2.5 magnitudes. The wind had thus transitioned from its cool optically thick state to a much less dense state in only 20 days. The spectrum at this time resembles the winds of some luminous, hot supergiants with high mass loss, and the spectra of some giant eruption LBVs or impostors such as SN2009ip (Smith et al 2010, Foley et al 2010).

The mean emission and absorption velocities for the four phases discussed here are summarized in Table 6.

4. Kinematics of the Ejecta

The measured Doppler velocities from the different emission line species (H, He I, Fe II), at any given phase, do not show any significant relative offsets. They are also consistent, within the errors, with the redshift of UGC 5460 at 1093 km s^{-1} throughout the eruption, although the Balmer emission lines show a progression to higher velocities with time, discussed below. There is no rotation curve for UGC 5460, so we do not know the expected velocity for SN2011ht. For this discussion, we therefore adopt the galaxy redshift as the intrinsic velocity for SN 2011ht. The velocities of the absorption lines, excluding the P Cygni-type absorption components altered by emission, are very uniform throughout the eruption with mean velocities at each phase of $\sim 530 - 560 \text{ km s}^{-1}$. The expansion velocity

of the circumstellar ejecta is thus $\sim 550 \text{ km s}^{-1}$, blueshifted relative to SN2011ht. Given the uncertainty in the intrinsic velocity, the expansion velocity is realistically between 500 and 600 km s^{-1} .

Only during the decline, when the ejecta had become optically thin, do we see a significant change in the velocities. Both the Ca II triplet and the [Ca II] emission lines show a statistically significant difference of $\approx 150 \text{ km s}^{-1}$ and 350 km s^{-1} , respectively, with respect to the hydrogen emission. As already mentioned the [Ca II] lines are formed in a very low density region which is thus moving outward relative to the object or the hydrogen emission region.

The velocity difference between the emission peaks and their corresponding absorption minima appears to increase with time from the hot wind stage to the decline, from about 560 km s^{-1} in the hot wind and transition phases to 640 km s^{-1} in the cool wind stage in both the hydrogen and the Ca II lines. The weak absorption minima in $\text{H}\alpha$ and $\text{H}\beta$ in the low density wind have a velocity difference as high as 700 km s^{-1} relative to the emission peaks. However, inspection of the velocities in Table 5 shows that this is actually due to an increase in the redshift of the emission lines suggesting a possible contraction of the ionization zone.

In the next section we show that the broad asymmetric wings are consistent with Thomson scattering and use the scattering model to estimate the outflow density and mass loss rate.

5. The Scattering Wings

The Balmer emission lines have the familiar characteristics of Thomson scattering in a dense outflow: roughly triangular profiles with concave sides, asymmetric to the red, and with wings extending much farther than one would expect from the absorption line velocities. The individual profiles for the $\text{H}\alpha$, $\text{H}\beta$ and $\text{H}\gamma$ are shown in Figure 8. The Doppler-shifted wings do not indicate bulk velocities, but are instead caused by multiple scattering events. Thomson scattering has at least two major implications: (1) There is no persuasive evidence for any outflow velocities much greater than about 600 km s^{-1} during the eruption, and (2) the line wings can be used to estimate the mass loss rate (see below). Additional support for this interpretation is presented in §5.1.

Dessart et al. (2009) convincingly demonstrated that similar asymmetric wings in SN1994W were due to Thomson scattering. Figure 11 in their paper, for example, shows a Thomson scattering model profile that closely resembles our Figure 8. For SN2011ht the strength of the scattering wings compared to line-center increases mildly from $\text{H}\alpha$ to $\text{H}\beta$

to $H\gamma$; qualitatively this effect is expected but it seems less conspicuous than in the case described by Dessart et al. (cf. their Fig. 12). The wavelength offsets and velocities corresponding to the Thomson scattering wings are summarized in Table 7 for $H\alpha$ and other lines. In SN2011ht, the wings also appear to become less extended at later times, presumably due to a decrease in the electron density and/or temperature. Since the ejecta are optically thick, we attribute this change primarily to a decrease in the apparent temperature and in τ_{sc} as the eruption progressed from the hot to cool wind phase. There are no apparent Thomson scattering wings on the $H\alpha$ and $H\beta$ emission profiles observed in the warm, thin wind during the decline when τ_{sc} is expected to be small.

5.1. The Balmer lines and the flow density

Adopting the Thomson scattering model for the broad wings in the Balmer lines, we can obtain simple order-of-magnitude estimates of the outflow densities and the mass loss rate. We employ a few very simplified assumptions that most likely resemble the true situation. When similar reasoning was applied to the case of η Car’s wind (Davidson et al 1995), the results were close to those found later with an elaborate wind model (Hillier et al 2001).

Consider a steady, constant-velocity spherical mass outflow with locally averaged electron density $\langle n_e(r) \rangle = \zeta/r^2$, where ζ is a constant parameter which we hope to estimate. In the simplest reasonable model, the emission line in question originates outside some radius r_1 , while at smaller radii the photons are presumably absorbed by continuum processes before they escape. In this case the emergent emission-line luminosity can be represented as a volume integral

$$L_{\text{line}} \approx \int A n_e^2 dV \approx \frac{4\pi A \zeta^2}{\epsilon r_1}, \quad (1)$$

where $\epsilon \leq 1$ is the standard “clumping factor” to allow for inhomogeneous densities. The emission rate parameter A is roughly known for each Balmer recombination line (Osterbrock & Ferland, 2006), except that continuum absorption and other effects reduce its effective value in a dense wind. Meanwhile the Thomson scattering optical depth at radius r_1 is

$$\tau_{sc} \approx \frac{\sigma_e \zeta}{r_1}. \quad (2)$$

If observations give estimates of L_{line} and τ_{sc} , we can eliminate r_1 to find the density parameter:

$$\zeta \approx \frac{\sigma_e \epsilon L_{\text{line}}}{4\pi A \tau_{sc}}. \quad (3)$$

With an adopted outflow speed, this gives an estimate of the mass loss rate. Various subtleties

which do not alter the basic reasoning have been omitted here. Note that the average emergent line photon originates around $\tau \sim 0.5\tau_{\text{sc}}$.

In this calculation we adopt the parameters measured for H β in the MODS1 spectrum from 2011 November 17. A Thomson-scattered line profile is broadened and shifted by the electrons' thermal motions (e.g., $v_e(\text{rms}) \approx 830 \text{ km s}^{-1}$ at $T = 15000 \text{ K}$) and by expansion of the outflowing gas. We can estimate τ_{sc} from the average number of scattering events before escape, which is indicated by the line broadening. Unfortunately the line width is not easy to parametrize in terms of observables, because the wings have no definite limits and the ill-defined, unscattered core of the line affects its central part. An acceptable measure for our purposes is

$$U_{\text{sc}} = \frac{\int |\lambda - \lambda_c| F(\lambda) d\lambda}{\int F(\lambda) d\lambda}, \quad (4)$$

where λ_c is the centroid of the emission line.² Thus we estimate $U_{\text{sc}} \approx 1850 \text{ km s}^{-1}$ for H β in 2011 November. If $v_e(\text{rms}) \approx 830 \text{ km s}^{-1}$ and the wind speed is 550 km s^{-1} based on the absorption features, then the estimated value of U_{sc} requires $\tau_{\text{sc}} \sim 3.5$. This estimate is based on Monte Carlo trials with the source distribution stated in eq. 1. It is inexact because the assumptions are simplified, and the central part of the line shape is not modeled realistically. The line wings, however, are represented better and would appear visibly different if τ_{sc} were less than 1.8 or more than 7. In the former case, the long-wavelength wing would be only a relatively weak satellite to the core of the line; while in a high- τ_{sc} case the profile would be dominated by the wings with no perceptible core. The range $1.8 \lesssim \tau_{\text{sc}} \lesssim 7$ spans a factor of two in U_{sc} .

The luminosity of H β in November 2011 was about $1.6 \times 10^{40} \text{ ergs s}^{-1}$. The parameter A in eq. 1 would have a value of about $10^{-25} \text{ erg cm}^3 \text{ s}^{-1}$ in a nebular case (Osterbrock and Ferland 2006), but absorption in the line formation region can somewhat reduce the effective emissivity; we tentatively adopt the value just quoted. Putting these quantities into eq. 3, we find $\zeta \sim 2 \times 10^{39} \epsilon \text{ cm}^{-1}$, which implies a mass-loss rate of the order of $0.05 \epsilon M_{\odot} \text{ y}^{-1}$ if $V_{\text{wind}} \approx 550 \text{ km s}^{-1}$. These values imply $r_1 \sim 30\epsilon \text{ AU}$, compared to a photosphere size of roughly 30 AU based on the continuum brightness (Paper I and §7 of this paper). In view of the uncertainties, this order-of-magnitude outcome appears satisfactory. In order to prevent r_1 from becoming implausibly small, evidently the clumping factor ϵ cannot be very small. Note that *our r_1 estimate for November 2011 is almost entirely independent of the photospheric size estimate, and it turns out to have the same order of magnitude.*

² The r.m.s. width, using $(\lambda - \lambda_c)^2$ instead of $|\lambda - \lambda_c|$, is theoretically more apt but in practice is too sensitive to the poorly measured extremities of the wings.

Another independent argument also appears consistent with the deduced mass loss rate. Davidson (1987) assessed the relation between mass loss rate and photosphere radius in an opaque wind with a given luminosity. Figure 1 in that paper is a plot of photospheric temperature vs. a relevant quantity Q which depends on mass loss rate, wind speed, and luminosity. The parameters quoted above for SN2011ht imply $\log Q \approx -5.5$, but in order to compensate for modernized opacities we should increase this to roughly -5.2 in that figure. *This value places the outflow near a critical part of the temperature vs. Q relation.* It is consistent with a photospheric temperature fairly close to 10^4 K as observed; and, more important, it also implies that either a moderate decrease in luminosity or a moderate increase in the mass loss rate would change the spectrum to a classic “cool dense wind” state. The character of the spectrum did indeed change in that way a few weeks later (§3.4). In summary, two very different modes of reasoning are both consistent with a mass loss rate of the order of $0.05 M_{\odot} \text{ y}^{-1}$ in 2011 November; and they are both consistent with the size of the continuum photosphere inferred from its brightness and color.

The Thomson broadening argument gives a less satisfactory result if we concentrate on $\text{H}\alpha$ rather than $\text{H}\beta$. With a nebular value of the emissivity A , $\text{H}\alpha$ seems to imply $r_1 \lesssim 20$ AU. However, self-absorption is much stronger for $\text{H}\alpha$ than for the other Balmer lines; so the effective value of A in the emission zone is likely to be substantially smaller than the nebular value, thereby eliminating the discrepancy. In any case, this discrepancy is no worse than the factor-of-two uncertainty expected for our simplified approximations. Higher Balmer lines appear satisfactory.

The size scale noted above, of the order of 30 AU for both continuum and emission lines, presents difficulties for any model with a massive supernova shock wave. The reasons will be outlined in §8 below.

Radiation pressure exceeded the Eddington Limit by perhaps two orders of magnitude in November 2011, but this has no bearing on the emergent-radiation analysis. Altogether, the case for Thomson scattering line wings is very strong. The observed profiles have the right shapes and widths (cf. Fig. 11 in Dessart et al. 2009), and the analysis based on this view leads to the same wind density as an entirely independent mode of reasoning as stated above. Moreover, the characteristic size of the relevant zone is found to be of the same order of magnitude as the photosphere estimated in Paper I. Any alternative hypothesis would need to explain all these facts. If SN2011ht was a true supernova, then it must have generated the protracted post-explosion low-speed dense outflow described above; and any faster shock wave must have escaped observation. If, on the other hand, SN2011ht was a different type of eruption, then the low-speed flow may have been the main event. Dynamical models of such an extreme super-Eddington case are beyond the scope of this paper.

Although the above reasoning is highly simplified, a full-fledged wind model like Dessart et al. (2009) may not improve the results as much as one might hope. The velocity and inhomogeneity functions $v(r)$ and $\epsilon(r)$ are scarcely known for a continuum-driven eruptive outflow; radiative transfer in the Balmer lines may have intricate local variations; the example of η Car shows that spherical symmetry can be a poor approximation, etc. In principle, these effects together imply that a standard wind-code model is valid for this type of object only in an order-of-magnitude sense – i.e., its derived quantities are only moderately more accurate than our simple approach.

A final point: The spectra of several Type II n supernovae show similar broad asymmetric wings in the Balmer lines (Kiewe et al 2012) which have been interpreted as due to actual mass motion, a mix of expansion and scattering, and as pure Thomson scattering. The wings in SN1994W have been demonstrated to be due to Thomson scattering, and in SN2011ht we have also shown that the behavior of the asymmetric wings is consistent with the expectations of Thomson scattering. *Therefore a word of caution is justified regarding similar asymmetric broad wings observed in several Type II n supernovae. Fitting these profiles with multiple Gaussians or other arbitrary distributions is very likely to lead to erroneous conclusions regarding the expansion velocities.*

6. The Later Spectral Energy Distribution and Dust Formation

SN2011ht’s visual brightness declined by 4.5 magnitudes in less than 25 days during January and February 2012 (Figure 1), and afterward significant flux was measured at $\lambda \sim 2$ to $4 \mu\text{m}$ (Figure 2). This near and mid-IR emission most likely indicates the presence of warm dust. In addition to the rapid decline, the visual photometry obtained at the end of the plateau phase (JD 5950.7, Table 1) compared with the post-decline photometry in Table 2 suggests that the object also got significantly redder. Its $b - v$ color of 0.65 mag immediately prior to the decline coincides with the cool wind phase and is consistent with the apparent spectral type and the low reddening derived in Paper I. The $ugri$ photometry measured 60 days later is equivalent to a redder $b - v$ color of $\sim 0.95 \text{ mag}^3$ and a color excess of $\sim 0.3 \text{ mag}$, relative to the pre-decline colors. This could be due either to dust formation or a continued shift in the energy distribution to cooler temperatures. Unfortunately, the only spectra we have for comparison during the decline show an unresolved continuum and

³The r -band magnitude is contaminated by $\text{H}\alpha$ emission (see Figure 2). Correcting for the $\text{H}\alpha$ flux gives a slightly fainter R magnitude of 20.1. Converting the $ugri$ photometry (Karaali, Blir & Tuncel 2005; Jester et al. 2005) yields a corresponding $b - v$ color of 0.95 - 0.99 mag.

emission lines (Figure 7). Assuming that the color excess is all due to dust formation with a normal reddening law, A_v is ~ 1.0 mag, with $R = 3.2$ and could account for about one-fourth of the decline in brightness. The color excess also implies a neutral hydrogen column density, n_{HI} , of $\approx 2.6 \times 10^{21}$. Unfortunately one cannot make a trustworthy estimate of the mass of the dust, because that would require several assumptions that are very doubtful in this case. (A precedent might be the η Car eruption, for instance; its grains and value of R are much larger than normal and the reasons are not understood, see references in Davidson and Humphreys 1997.)

Dust has been confirmed in several Type II_n's which somewhat distinguishes them from other supernovae (Fox et al. 2011, Otsuka et al. 2012). Similar objects that declined rapidly and then were observed later to have formed dust include SN2007od, SN2009kn, and SN1994W (Sollerman et al. 1998, Andrews et al. 2010, Kankare et al. 2012), all similar to SN2011ht. In these cases the rapid luminosity decrease was said to imply a very low mass of radioactive ^{56}Ni in the ejecta. Few authors take this idea to its logical limit: perhaps the event was not a core-collapse SN, hence no ^{56}Ni (cf. Dessart et al. 2009). Thus the presence of dust is potentially significant and the near-IR flux is worth examining, even though theoretical difficulties preclude any satisfying model for the dust with the limited information we have.

Only a small fraction of the observed near-IR flux can be thermal free-free emission. In order to match the $\lambda \sim 2 \mu\text{m}$ flux (Figure 2) with this mechanism, a mass loss rate of the order of $0.01 M_{\odot} \text{ y}^{-1}$ is required. Intuitively this rate seems higher than one would expect for January 2012, since it is nearly of the same order of magnitude as the value estimated in §5 above for an early, much more active stage of the event. Concrete objections to the free-free hypothesis are as follows. The resulting λF_{λ} would rise toward smaller wavelengths more than was observed, and the emission lines should be much stronger than those shown in Figure 7. Thus we can reasonably assume that the 2–4 μm flux originates chiefly from scattering and emission by warm dust grains rather than thermal bremsstrahlung. The central object's continuum plus bremsstrahlung may account for an appreciable fraction at $\lambda \lesssim 2 \mu\text{m}$, however.

If, for example, 70% of the 2 μm flux and all of the 4 μm flux were emitted by grains, then the 2–4 μm spectral slope in Figure 2 corresponds to a dust temperature of roughly 900 K – presumably an average over a range of grain temperatures.⁴ Figure 2 indicates an

⁴ With a typical absorption efficiency function, the wavelength distribution of emission from a small grain at $T = 900$ K resembles a 1100 K blackbody. We mention this because some authors have used Planck curves to represent observed dust SED's.

integrated luminosity of about $6 \times 10^6 L_\odot$ for SN2011ht in March 2012, about $100\times$ less than it was three months earlier. With this value, a grain absorption efficiency proportional to λ^{-1} (Draine 2011), and a source color temperature around 6000 K, the distance from the star corresponding to dust temperature T_d is

$$r \approx (500 \text{ AU}) (T_d/1000 \text{ K})^{-2.5}. \quad (5)$$

If the stated assumptions are close to reality, the observed near-IR in Figure 2 originated mainly at locations 400 to 1000 AU from the central object. At a speed of 550 km s^{-1} , the material in question would have been ejected 3–10 years before the event. This idea seems basically reasonable, since a pre-event mass loss rate less than $10^{-3} M_\odot \text{ y}^{-1}$ would have given a sufficient column density in the region $r \gtrsim 400 \text{ AU}$.

However, the same reasoning leads to a grain-formation puzzle. During the high-luminosity stages of the event, dust should have been heated to temperatures roughly $2.5\times$ higher, averaging about 2300 K instead of 900 K – probably hot enough to destroy pre-existing grains. Thus, at first sight, it seems likely that new grains formed as the luminosity declined in early 2012. But at a gas density of the order of 10^{-19} or $10^{-18} \text{ g cm}^{-3}$ (consistent with the above remarks), a grain cannot grow to a size of, say, $0.01 \mu\text{m}$ in only 2 months via simple accretion of thermal atoms (Kochanek 2012). The shortfall in growth rate is two or three orders of magnitude. We do not have a satisfying answer to this paradox, but note the following considerations:

1. One can speculate that the relevant gas at $r \sim 500 \text{ AU}$ was compressed by a shock wave plus subsequent cooling e.g., in a true SN explosion. However, in order to reach the radius of interest only half a year after the initial explosion, the shock speed must have been several thousand km s^{-1} , which implies a post-shock temperature above 10^8 K and a cooling time of many years in the relevant gas – so the compression factor would not have been very much larger than the adiabatic value 4, insufficient to explain the phenomenon, while the high temperature would create an environment hostile to dust. In any case, deducing a strong shock wave from the near-IR flux alone would be an extreme extrapolation.
2. It is not certain that all the relevant pre-existing grains were destroyed by the maximum luminosity. The 2012 near-IR flux might have been produced by slightly cooler dust than we estimated above, and parts of especially refractory grains may have survived up to 2000 K or so. The unidentified bands (§3.1) may be relevant to this question. They could be remnants of previous existing circumstellar material.

3. The grains might grow faster than the very simple estimate quoted above. If the pre-eruption wind speed was of the order of 100 km s^{-1} rather than 550 km s^{-1} (i.e., like a cooler hypergiant or an LBV at maximum), or if the outflow is inhomogeneous, then local density maxima at $r \sim 500 \text{ AU}$ could have greatly exceeded $10^{-18} \text{ g cm}^{-3}$. Meanwhile, radiation-driven motion of the grains through the gas might cause faster growth; and of course there may be other processes that we have not thought of.

4. Consider the near-IR flux of $\eta \text{ Car}$, a well-observed object with practically the same luminosity and wind speed that SN2011ht had in March 2012. In 1970–2000 $\eta \text{ Car}$'s mass loss rate was of the order of $10^{-3} M_{\odot} \text{ y}^{-1}$ (Davidson & Humphreys 1997, Hillier et al. 2001).⁵ Based on simple accretion of thermal atoms, one would predict that the radius of a grain 500 AU from $\eta \text{ Car}$ would initially grow no faster than about $3 \times 10^{-4} \mu\text{m y}^{-1}$, and this rate would decrease within 3 years as the grain moves outward. This is too slow to produce much near-IR emission in $r \lesssim 1000 \text{ AU}$. In fact a 2–5 μm continuum was observed and we can interpret its spectral slope, as follows. First consider an idealized spherical, constant-velocity outflow. Suppose that the absorption coefficient of dust in this outflow has radial dependence $k(\nu, r) \propto r^{-\alpha}$. (Thus $\alpha = 2$ means that the extinction per unit mass is constant.) If $T(r) \propto r^{-0.4}$ and $kr \ll 1$, one can show that near-IR emission from the dust has frequency dependence $f_{\nu} \propto \nu^{2.5\alpha-3.5}$. The observed 2–5 μm spectrum of $\eta \text{ Car}$ in 1970–2000 closely resembled $f_{\nu} \propto \nu^{-3.8}$ (see, e.g., Figure 3 in Cox et al. 1995). Roughly speaking, this suggests $k \propto r^{0.1}$ at radii $r \approx 500$ to 2000 AU . In other words, the amount of dust extinction per unit overall mass appears to have grown substantially in a flow time of 10 years or even 5 years – contrary to the simple expectation quoted above. Evidently the well known example of $\eta \text{ Car}$ presents the the same near-IR puzzle as SN2011ht. One can imagine potential pitfalls in this analysis, but it illustrates that the theoretical grain-formation problem is not strong enough to invalidate our basic view of SN2011ht's post-eruptive state. The same problem exists even if the event was a true supernova.

7. The Stellar Wind, Circumstellar Ejecta, and Mass Loss

SN2011ht is remarkably similar to SN1994W and to SN2009kn which has recently been described as a spectroscopic twin to SN1994W (Kankare et al. 2012). These objects and similar Type IIn's have been assumed to be true supernovae of either Type IIn or Type IIP

⁵ We cite old estimates because $\eta \text{ Car}$'s wind density has considerably decreased since 2000 (Mehner et al. 2010, 2012; Martin et al. 2006).

in which the shock from the terminal explosion interacts with a previously existing dense circumstellar medium. Dessart et al. however have suggested that SN1994W’s spectroscopic evolution and luminosity can just as well be explained as the collision of two shells or ejections. The principle difference in the observational record between SN2011ht and these other Type IIn’s is the *Swift* near-UV photometry for SN2011ht. If UV observations had been available for SN1994W, we suspect that it likewise would have had a strong UV flux in its early hot wind phase.

In this section we begin by discussing the physical parameters of SN200ht’s wind or ejecta that can be derived from its spectra and light curve.

The discovery spectrum described by Pastorello et al (2011) showed a forest of Fe II absorption lines, Ba II and Ca II H and K in absorption, and hydrogen and the Ca II triplet in emission with P Cygni profiles. Although we do not have a copy of the spectrum, this description is consistent with the “F-type” supergiant spectrum observed in several giant eruption LBVs and in the warm hypergiants. Adopting an apparent temperature of ~ 7000 K with SN2011ht’s luminosity of $M_v = -14.4$ mag at that time, the ejecta or dense wind had a radius of only 20 AU. If this material is expanding at 550 km s^{-1} , it would have reached this distance ≈ 0.2 yr prior to the discovery.

During the hot wind phase when the UV flux was a maximum in mid-November 2011, the apparent temperature of the dense wind was $\sim 13000^\circ\text{K}$ (Paper I). The total luminosity at that time was $10^9 L_\odot$ and the corresponding photospheric radius was 30 AU. In §5.1, we estimated a mass loss rate on the order of $0.05 M_\odot \text{ y}^{-1}$ from a model for the scattering wings in the Balmer lines in this phase. This is much below what we would expect for a terminal explosion and much higher than in the classical LBVs at maximum which typically have mass loss rates of 10^{-4} to $10^{-5} M_\odot \text{ y}^{-1}$ (Humphreys & Davidson 1994).

As the total luminosity declined and the UV flux decreased, the apparent temperature of the wind decreased fairly rapidly as observed in the transition spectra, and the photosphere moved outward into the ejecta. In the cool dense wind phase the absorption lines correspond to a late-F/early G-type supergiant. Adopting an apparent temperature of $\sim 6000 - 6500^\circ\text{K}$ and a luminosity of $1.6 \times 10^8 L_\odot$, the photospheric radius was 50 - 60 AU. With an expansion velocity of 550 km s^{-1} , the ejecta would have reached this distance in about 6 months. The temperature was very likely higher in the preceding warm phase because the dense ejecta had not moved far enough out for a cool photosphere.

The expansion velocity measured from the absorption lines throughout the eruption is $\sim 550 \text{ km s}^{-1}$ with some material up to $\sim 700 \text{ km s}^{-1}$. The corresponding times for the ejecta to reach the above radii imply pre-existing ejecta and an earlier or on-going eruption

only shortly before the discovery. The pre-outburst upper magnitude limit from Boles (2011) at ~ 19.5 mag in April, 2011, also restricts the previous outburst to no more than 0.5 yr before the discovery, unless the initial outburst had already begun at that time.

The transition to the thin wind stage during the decline was accompanied by the appearance of the [Ca II] lines which are relatively rare and require very low densities. Furthermore, the Balmer emission lines show no evidence of the Thomson scattering wings which had dominated their line profiles in the earlier spectra. Both of these observations suggest that the optical depth and electron density greatly decreased. Since the hydrogen emission line profiles are no longer distorted by the strong wings, the FWHM of the H α emission line measured at 900 km s^{-1} may be indicative of the corresponding wind speed. Although the few absorption lines present in the spectrum still indicate an outflow velocity of $\sim 550 \text{ km s}^{-1}$, we identify this higher velocity with a possible increase in speed and decrease in density of the outflow. At this velocity, the wind would have caught up with the slower expanding ejecta and reached the 50 AU photospheric radius of the cool dense wind in about 120 days, or at about the time the rapid decline began. We suggest that this transition corresponds to when the ejecta becomes optically thin. The faster wind may thus be associated with a second eruption as suggested for SN1994W (Dessart et al. 2009).

8. Discussion – Supernova or Impostor?

SN2011ht has been called both an impostor and a true supernova. With its high visual luminosity at maximum it is tempting to assume that it was a terminal explosion, but there are serious contradictions with the standard expectations for supernovae. SN2011ht exhibited relatively modest outflow velocities and a total detected energy release that seem more appropriate for a non-supernova giant eruption.

Integrating over SN2011ht’s multi-wavelength light curve, the luminous energy emitted from discovery to the onset of the decline was roughly 2.5×10^{49} ergs. The kinetic energy based on our mass-loss estimates would be much smaller. Additional mass loss is possible, but at speeds around 600 km s^{-1} , even $10 M_{\odot}$, for example, would carry less than 4×10^{49} ergs. *There is no evidence for substantially higher velocities in any of our spectra before the decline*, and later only moderately faster values in small amounts of material. The data therefore strongly suggest $E < 10^{50} \text{ km s}^{-1}$, an order of magnitude less than a supernova’s typical kinetic plus luminous output. The observed amount of energy is present in the outer parts of a massive hot star, if a suitable instability exists to make it available.

The analysis in §5.1 presents difficulties for a hypothetical massive SN blast wave. Three

different modes of reasoning all led to a characteristic size of 30–60 AU for both the continuum and the hydrogen emission lines, during a two-month interval around maximum brightness. The inferred mass in the emission region was then small, $M_{\text{em}} \ll 1 M_{\odot}$. An initial blast wave faster than 1500 km s^{-1} would have passed that radius several weeks earlier. In that case, one must explain why the hypothetical massive shock did not heat the observed gas and sweep it away. If the spectra represent successive inner layers following a blast wave outward, then why did the observed velocity remain fairly constant? (A simple model would predict a continuously decreasing velocity, resembling a Hubble flow. Naively, at least, the hydrogen-rich spectrum also seems a little surprising for inner layers of a SN outflow.) Generally speaking, the observed behavior looked like a continuous, moderate-mass outflow from a fixed center, i.e., from a surviving star.

A true SN may be able to evade the above objections *by strongly departing from spherical symmetry*. Conceivably the main shock wave and kinetic energy were restricted to a range of spatial directions, with slower outflows in other directions. One can imagine either an axially symmetric explosion (pictorially resembling a GRB and/or η Car), or a fully asymmetric event. With axial symmetry, for instance, our observations might refer to equatorial material while a massive shocked polar outflow was too hot to see. We cannot develop this possibility here, but it has relevance to Type II_n supernovae in general.

As an anonymous referee comments, an electron-capture supernova has been proposed by some authors (Botticella et al. 2009; Thompson et al. 2009) to explain the less luminous outbursts from lower mass stars such as the ILRTs. Although a wide range of masses are possible for the progenitor based on the constraints discussed in Paper I, there is no observational information that the progenitor of SN2011ht was a lower mass star. Its light curve and spectral evolution differ from the ILRTs. The electron-capture idea may be possible, but it is essentially a conjecture, presupposing the event to have been a supernova, and not based on any clear implications from the data. Arguments for an unfamiliar type of SN based on the light curve are intrinsically weak, because there is no obvious discrepancy between the observed shape and a non-SN eruption. Spectroscopy is more critical.

The presence of X-ray emission identified with SN2011ht in Paper I initially appeared to support a supernova interpretation. Although there was no significant X-ray flux measured at early times with the *Swift* X-Ray Telescope, it was reported later. This later measurement however is now in doubt. Observations with *Chandra* apparently do not confirm that SN2011ht was the X-ray source (Pooley 2012). Although, strictly speaking, X-rays indicate a supernova only indirectly. Giant eruptions may also have shocks and X-rays.

In this paper we have emphasized the lack of clear evidence for high velocities in SN2011ht’s eruption; but even if a shock wave occurred, it need not have been a *blast wave*

resulting from a central explosion. When super-Eddington radiation drives an eruption like giant outbursts or η Car, the material automatically becomes inhomogenous (Owocki & Shaviv 2012). Material in at least the lower-density regions can be accelerated to supersonic speeds. As Davidson (2012) remarked, one consequence might be a shock at the beginning of the eruption, which in principle can accelerate outward through the decreasing density gradient of pre-eruption material. In order to verify a true core-explosion SN (a bona fide shock wave formed near the center), the shock must be one or two orders of magnitude more massive and energetic than anything seen directly in SN2011ht. Perhaps it really was a terminal explosion, but if so the main SN kinetic energy was remarkably inconspicuous.

The steep declines observed in the light curves of SN1994W and SN2009kn have been attributed to a very low production of ^{56}Ni , assuming that they were true supernovae. We observe a similar steep decline in SN2011ht which by analogy would imply an equally low amount of ^{56}Ni . Indeed, Dessart et al. used this low result ($0.0026 - 0.015M_{\odot}$, Sollerman et al. 1998) to also infer that SN1994W might not be a terminal explosion. If the event was not really a supernova, then no ^{56}Ni is expected. Although dust formation was also observed in these two objects plus other Type IIn's, in SN2011ht we detected the dust relatively early. The integrated luminosities from the SEDs at later times indicate that the bolometric luminosity was decreasing rapidly and the eruption was ending. The decrease in the luminosity would have facilitated the formation of dust. In §6 we showed that dust formation might account for \sim one-fourth of the decline. The decline was thus likely due to a combination of the cessation of the eruption accompanied by dust formation. The eruption therefore lasted about one year. Identifying the post-decline brightness level (Figure 1) with radioactive decay would constitute another assumption, not a clear deduction, since a giant eruption object can produce some post-event light without radioactivity (e.g., η Car did).

Some of the above comments may also relate to other outbursts labeled as Type IIn supernovae. To explain the narrow emission lines and their high luminosities, most authors assume that the terminal eruption collides with a previously existing circumstellar medium ejected in events that occurred years before the SN, sometimes many years earlier. CSM of that type should be located hundreds or thousands of AU from the star. But Thomson-scattering line profiles combined with moderately hot continua seem more appropriate for size scales less than 300 AU, and less than 100 AU in most cases – less than a year of travel time for the outflowing gas. This casts some doubt on the concept of separate events in some of the objects. Indeed in several of these examples, especially SN1994W, SN2009kn, etc., the previous eruption is interestingly proposed to occur only about one year prior to the supernova explosion. In Paper I we suggested the same model for SN2011ht. If these objects are in fact supernovae, could this prior eruption be related to an interior instability just before the terminal eruption, or is this an example of the pulsational pair instability

that may occur in very massive stars? The “supernova impostors”, or giant eruptions, are spectroscopically very similar to the Type II n ’s. The primary distinction is the luminosity at maximum (see Van Dyk and Matheson 2012 for a review and references therein). So these objects could be examples of giant eruptions in which the high luminosity is due to interacting ejecta from two non-terminal eruptions as suggested by Dessart et al. for SN1994W. In the case of SN 2011ht, the observations are consistent with *one continuous outflow event* that began early in 2011 and grew rapidly after September. Since there is no clear theoretical model for giant eruptions, we cannot exclude the possibility of high visual brightnesses.

Motivated by the velocities and observable energy, we suggest that SN2011ht may have been a giant eruption driven by super-Eddington radiation pressure. The fact that it exceeded the Eddington Limit by a large factor is not a fatal objection, because (1) adequate theory has not been developed, and (2) the data strongly suggest that a hyper-Eddington flow did in fact exist for many weeks, independent of the cause (§3 and §5 above). Our observations and its pre-eruption record suggest the onset of an eruption only about 6 months before the discovery. SN2011ht was thus an ongoing high mass loss episode with an initial outburst that produced the slower, denser ejecta. The faster, lower density wind may be identified with a second outburst or an accelerated wind responsible for the post discovery visual and UV brightening. As already noted the post-plateau spectrum, dominated by the faster wind or ejecta, closely resembles the spectra of several giant eruption objects.

Thus SN2011ht and its twins, SN1994W and SN2009kn, bring into question the nature of the Type II n supernovae, or at least some of them. The true measure of a supernova is a terminal explosion, while for an impostor, the star survives. The likely progenitor of SN2011ht however was very faint with an upper magnitude limit at $g = 22.8$ mag (Paper I) which together with the current formation of dust, makes it unlikely we will observe the survivor, if it exists, for some time. If SN2011ht was a true supernova, then the eruption must have been quite non-spherical to separate the unseen blast wave from the gas that was observed.

It is a pleasure to thank the Directors of the Space Telescope Science Institute and the Gemini Observatory for their allotment of Director’s Discretionary Time for the STIS/MAMA and NIRI observations with *HST* and Gemini-North, respectively. This paper uses data taken with the MODS spectrographs built with funding from NSF grant AST-9987045 and the NSF Telescope System Instrumentation Program (TSIP), with additional funds from the Ohio Board of Regents and the Ohio State University Office of Research. R. Humphreys thanks Perry Berlind and the MMT staff for the Hectospec spectra and Luc Dessart for useful comments on Thomson scattering profiles. We also thank Peter Roming for providing the later data from *Swift* and Chris Kochanek for useful remarks on an early draft of this

paper. Research on massive stars by R. Humphreys and K. Davidson is supported by the National Science Foundation AST-1019394.

Facilities: LBT/MODS1, MMT/Hectospec, HST/STIS, LBT/Lucifer, GEMINI/NIRI

REFERENCES

- Andrews, J. E., et al. 2010, ApJ, 715, 541
- Berger, E. et al. 2009, ApJ, 699, 1850
- Boles, T. 2011, CBET 2851
- Bond, H. E., Bedin, L. R., Bonanos, A. Z., Humphreys, R. M., Monard, L. A. G. B., Prieto, J. L., & Walter, F. M. 2009, ApJ, 695, L154
- Botticella, M. T., et al. 2009, MNRAS, 398, 1041
- Chugai, N. N. 2001, MNRAS, 326, 1448
- Chugai, N. N. et al. 2004, MNRAS, 352, 1213
- Cox, P., Mezger, P.G., Sievers, A., Najarro, F., Bronfman, L., Kreysa, E., & Haslam, G. 1995, A&A, 297, 168
- Davidson, K. 1987, ApJ, 317, 760
- Davidson, K., Ebbets, D., Weigelt, G., Humphreys, R. M., Hajian, A. R., Walborn, N. R. & Rosa, M. 1995, AJ, 109, 1784
- Davidson, K., & Humphreys, R.M. 1997, Ann. Revs. Astr. Astrophysics 35, 1
- Davidson, K. 2012, in *Eta Carinae and the Supernova Impostors*, Astrophys. & Sp. Sci. Library 384 (ed. K. Davidson & R.M. Humphreys, Springer Media, New York), 43
- Dessart, L., Hillier, D. J., Gezari, S., Basa, S. & Matheson, T. 2009, MNRAS, 394, 21
- Draine, B.T. 2011, *Physics of the Interstellar and Intergalactic Medium* (Princeton University Press)
- Foley, R. J., et al. 2011, ApJ, 732, 32
- Fox, et al. 2011, ApJ, 741, 7

- Hillier, D. J., Davidson, K., Ishibashi, K. & Gull, T. 2001, ApJ, 553, 837
- Humphreys, R.M.& Davidson, K. 1994, PASP, 106, 1025
- Humphreys, R.M., Bond, H. E., Bedin, L. R., Bonanos, A. Z., Davidson, K., Monard, L.A.G. B., Prieto, J. L. & Walter, F. M. 2011, ApJ, 743, 118
- Humphreys, R.M. 2012, The Astronomer's Telegram, 3895
- Hurst, G. 2012, private communication
- Jester, S., et al. 2005, AJ, 830, 173
- Kankare, E. et al. 2012, MNRAS
- Karaali, S., Bilir, S., & Tuncel, S, 2005, Publ. Astron. Soc. Aust., 22, 24
- Kiewe, M. et al. 2012, ApJ, 744, 10
- Kochanek, C. 2012, private communication
- Martin, J.C., Davidson, K., & Koppelman, M.D. 2006, AJ, 139, 2056
- Mehner, A., Davidson, K., Humphreys, R.M., Martin, J.C., Ishibashi, K., Ferland, G.J., & Walborn, N.R. 2010, ApJ, 717, L22
- Mehner, A., Davidson, K., Humphreys, R.M., Ishibashi, K., & Martin, J.C. 2012, ApJ, 751:73
- Ofek, E. O., et al. 2010, ApJ, 724, 1396
- Osterbrock, D. F. & Ferland, G. F. 2006, *Astrophysics of Gaseous Nebulae and Active Galactic Nuclei* University Science Books
- Otsuka, M. et al. 2012, ApJ, 744, 26
- Owocki, S., & Shaviv, N. 2012, in *Eta Carinae and the Supernova Impostors*, Astrophys. & Sp. Sci. Library 384 (ed. K. Davidson & R.M. Humphreys, Springer Media, New York), 275
- Pastorello, A., Stanishev, V., Smartt, S. J., & Fraser, M. 2011, CBET 2851
- Pooley, D. 2012, The Astronomer's Telegram, 4062
- Prieto, J. L., et al. 2011, The Astronomer's Telegram, 3749

- Prieto, J. L., McMillan, R., & Bakos, G. 2011, CBET 2903
- Roming, P. W. A., Pritchard, T.A., & Brown, P. 2011, ATel 3690
- Roming, P. W. A. et al. 2012, ApJ, 751:92 (Paper I)
- Smith, N., et al. 2009, ApJ, 697, 49
- Smith, N., et al. 2010, AJ, 139, 1451
- Sollerman, J., Cuming, R. J., & Lundquist, P. 1998, ApJ, 493, 933
- Thompson, T., Prieto, J. L., Stanek, K. Z., Kistler, M. D., Beacom, J. F. & Kochanek, C. S. 2009, ApJ, 705, 1364
- Van Dyk, S. D. and Matheson, T. 2012, in *Eta Carinae and the Supernova Impostors*, Astrophys. & Sp. Sci. Library 384 (ed. K. Davidson & R.M. Humphreys, Springer Media, New York), 249

Table 1. *Swift* UVOT Late Times Photometry of SN 2011ht

Date UT JD2450000+	Day ^a	Observed Magnitudes ^b					
		<i>uvw2</i>	<i>uvm2</i>	<i>uvw1</i>	<i>u</i>	<i>b</i>	<i>v</i>
5950.7	117	19.96(29)	19.95(**)	18.18(12)	16.79(08)	16.15(07)	15.50(07)
5974.8	141	21.35(**)	21.33(**)	20.82(47)	20.69(**)	21.07(**)	20.02(49)
5981.9	148	21.82(**)	21.79(**)	21.25(45)	21.15(**)	21.51(**)	20.23(39)
5989.5	156	21.52(**)	21.49(**)	21.15(**)	20.84(**)	21.19(**)	20.31(**)
5991.4	158	21.69(**)	21.66(**)	21.34(**)	21.02(**)	21.37(**)	20.48(**)

^aThe day number since discovery on 29 September 2011 (Boles et al 2011).

^bValues in parenthesis are the errors. 3σ upper limits are marked with **.

Table 2. Late Times Visual and Infrared Magnitudes

JD	Day	u	g	r	i	J	H	K_s	L'	M'
5999.6	166	18.4 ± 0.15	17.4 ± 0.10	16.5 ± 0.10
6011.9	178	23.0 ± 0.5	20.9 ± 0.2	19.9 ± 0.2	20.0 ± 0.2
6050.2	217	17.0 ± 0.2	15.3 ± 0.15	>14.3

Table 3. Journal of Spectroscopic Observations

Instrument	Date (UT)	Day	Integration (sec)	Comment/Stage ^a
LBT/MODS1	2011-11-17	49	900	Hot wind
LBT/MODS1	2011-11-23	55	900	Hot wind
HET/LRS	2011-12-21	83	600	Transition
LBT/MODS1	2011-12-26	88	900	Transition
STIS/MAMA	2011-12-26	88	400	G230L/NUV2376
STIS/MAMA	2011-12-26	88	400	G230M/NUV2800
STIS/MAMA	2011-12-26	88	600	G140L/FUV1425
LBT/MODS1	2011-12-28	90	900	Transition
ARC/DIS	2012-01-02	95	600	Transition
ARC/DIS	2012-01-19	112	700	Cool wind
MMT/Hectospec	2012-01-23	116	900	Cool wind
MMT/Hectospec	2012-02-13	137	900	Decline
ARC/DIS	2012-02-22	146	900	Decline
ARC/DIS	2012-02-28	152	1200	Decline

^aSee §4

Table 4. Radial Velocity Summary for SN2011ht - hot wind phase^a

Identification	Emission km s ⁻¹	Absorption km s ⁻¹	Difference km s ⁻¹
Hydrogen			
H α	926	384	542
H β	950	429	521
H γ	995	470	525
H δ	1046	490	556
H ϵ	1096	514	582
H 8	1072	532	540
mean	1014 \pm 62	...	544 \pm 20
H 9	...	540	...
H10	...	569	...
H11	...	565	...
H12	...	552	...
H13	...	530	...
H14	...	556	...
H15	...	598	...
mean	...	558 \pm 20	...
Helium			
λ 7065	955
λ 6678	1033	615	418
λ 5876	1041	567	474
λ 5016	1116	646	470
λ 4922	1082	695	387
λ 4471	976	610	366
λ 4026	...	633	...
λ 3819	...	597	...
mean	1033 \pm 56	615 \pm 17	423 \pm 43
Other			
Ca II K	...	564	...
O I λ 7774	...	529	...

^aline indentifications and Doppler velocities measured from the MODS1 spectrum from 17 Nov. 2011.

Table 5. Radial Velocity Summary for SN2011ht Post-Maximum Spectra

Identification	Emission km s ⁻¹	Absorption km s ⁻¹	Difference km s ⁻¹
<i>Transition</i> ^a			
Hydrogen			
H α	928	338	590
H β	962	370	592
H γ	947	435	512
H δ	1031	468	563
H ϵ	1073
H 8	1072	509	563
H 9	1103	548	555
mean	1017 \pm 65	...	563 \pm 26
H 10	...	561	...
H 11	...	557	...
H 12	...	528	...
H 13	...	595	...
mean	...	560 \pm 24	...
Other			
Ca II K	...	511	...
Ca II H	...	522	...
Fe II	1075 \pm 61 (8)	522 \pm 31 (8)	593 \pm 62 (7)
O I λ 7774	...	536	...
O I λ 8446	...	529	...
Ca II λ 8498	...	593	...
Ca II λ 8542	1117	527	590
Ca II λ 8662	1036	554	482
mean	1076 \pm 57	528 \pm 32	580 \pm 65
<i>Cool Wind</i> ^b			
Hydrogen			
H α	992	329	663
H β	1086	426	660
H γ	1057	470	587
H δ	1156	490	666
mean	1073 \pm 59	...	644 \pm 33
Other			

Table 5—Continued

Identification	Emission km s ⁻¹	Absorption km s ⁻¹	Difference km s ⁻¹
Ca II K	...	473	...
Ca II H	...	555	...
Fe II	1104 ± 22 (3 lines)	554 ± 25 (4 lines)	589 (2 lines)
Na I D	1158	445	713
O I λ7774	...	525	...
O I λ8446	...	494	...
Ca II λ8498	1144	470	674
Ca II λ8542	1113	436	677
Ca II λ8662	1091	436	655
mean	1116 ± 23	533 ± 35	637 ± 40
<i>Warm Thin Wind^c</i>			
Hydrogen
Hα	1070	315	755
Hβ	1123	432	691
Hγ	1182	470	712
mean	1125 ± 46	...	719 ± 26
Hδ	...	527	...
Hε	...	540	...
Other			
Na I D	1285	430	855
Fe II	1158 ± 34 (4 lines)
[Ca II] λ7291	732
[Ca II] λ7324	772
O I λ8446	959
Ca II λ8498	971
Ca II λ8542	962
Ca II λ8662	935

^aine indentifications and Doppler velocities measured from the MODS1 spectrum from 26 Dec. 2011.

^bDoppler velocities are the average from the ARC and MMT/Hectospec spectra from 19 Jan. and 23 Jan.2012.

^cDoppler velocities are the average from the ARC and MMT/Hectospec spectra from 13 Feb., 22 Feb., and 28 Feb. 2012.

Table 6. Emission and Absorption Velocity Summary

Stage	Balmer Em. km s ⁻¹	He I Em. km s ⁻¹	Other Em. km s ⁻¹	P Cyg Abs Difference km s ⁻¹	Absorption km s ⁻¹
Hot Wind	1014±62	1033±56	...	544±20	556±20
Transition	1017±65	...	1076±57	580±65	528±33
Cool Wind	1073±59	...	1116±23	640±37	533±35
Thin Warm Wind	1125±46	...	1172±28 ^a	719±26	534±6

^aNot including Ca II and [Ca II]. See Table 5 and §5.

Table 7. The Thomson Scattering Wings

Identification	Blue Wing $\Delta\lambda(\text{\AA})$	Blue Wing km s ⁻¹	Red Wing $\Delta\lambda(\text{\AA})$	Red Wing km s ⁻¹
<i>Hot Wind</i> (17 and 23 November 2011)				
H α	-105	-4726	+174	7939
He I λ 7065	-61	-2584	+86	3636
He I λ 5876	-58	-2936	+108	5490
<i>Transition</i> (26 and 28 December 2012)				
H α	-55	-2518	+102	4637
<i>Cool Wind</i> (19 and 23 January 2012)				
H α	-56	-2549	+73	3319
Ca II λ 8542	+28	987
Ca II λ 8662	+26	903

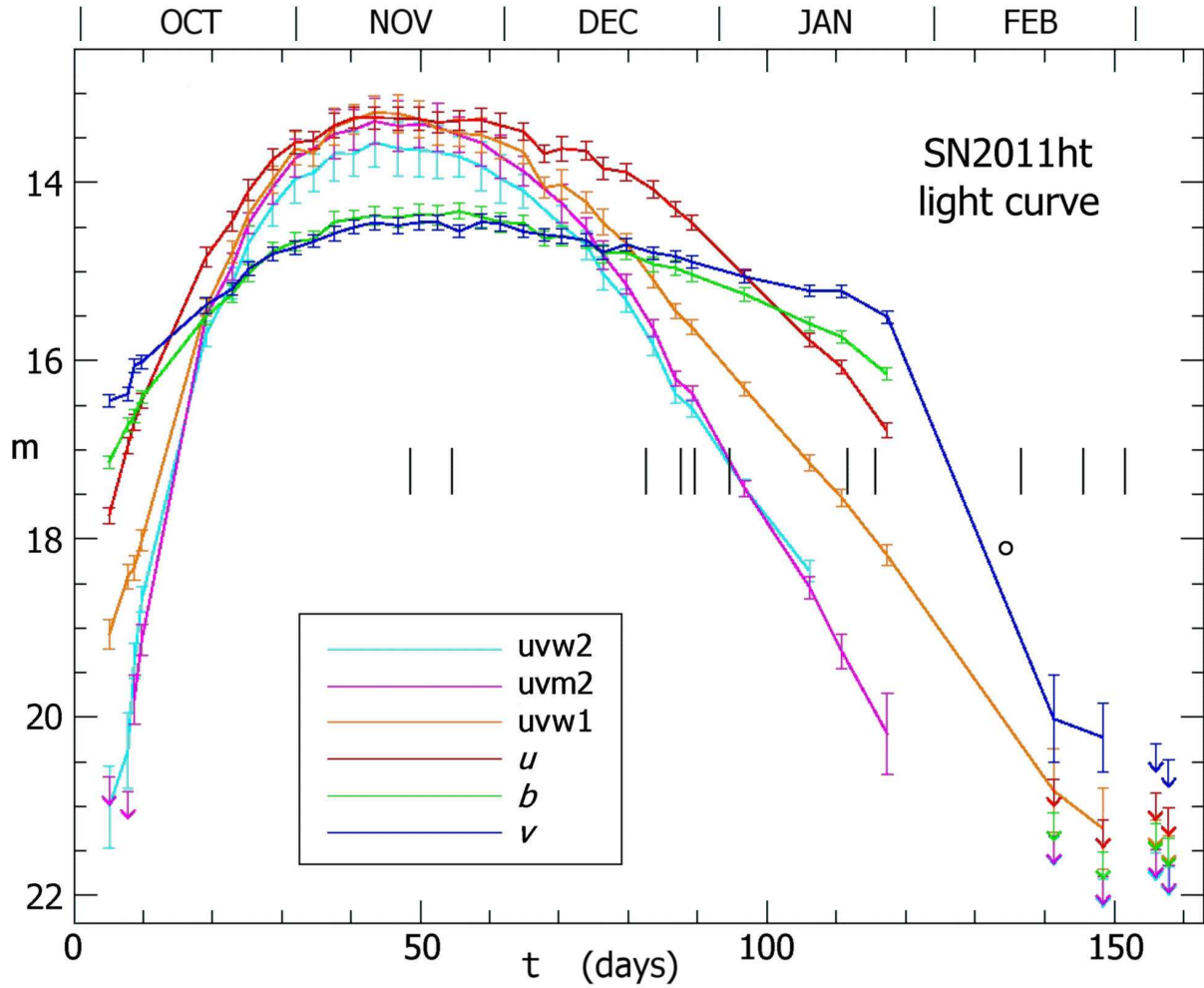


Fig. 1.— The *Swift* light curve. The zero-point for t is MJD 55833 = 2011 September 29. The tic marks show the times of the spectra discussed in this paper. The open circle is an approximate V magnitude from Hurst (2012).

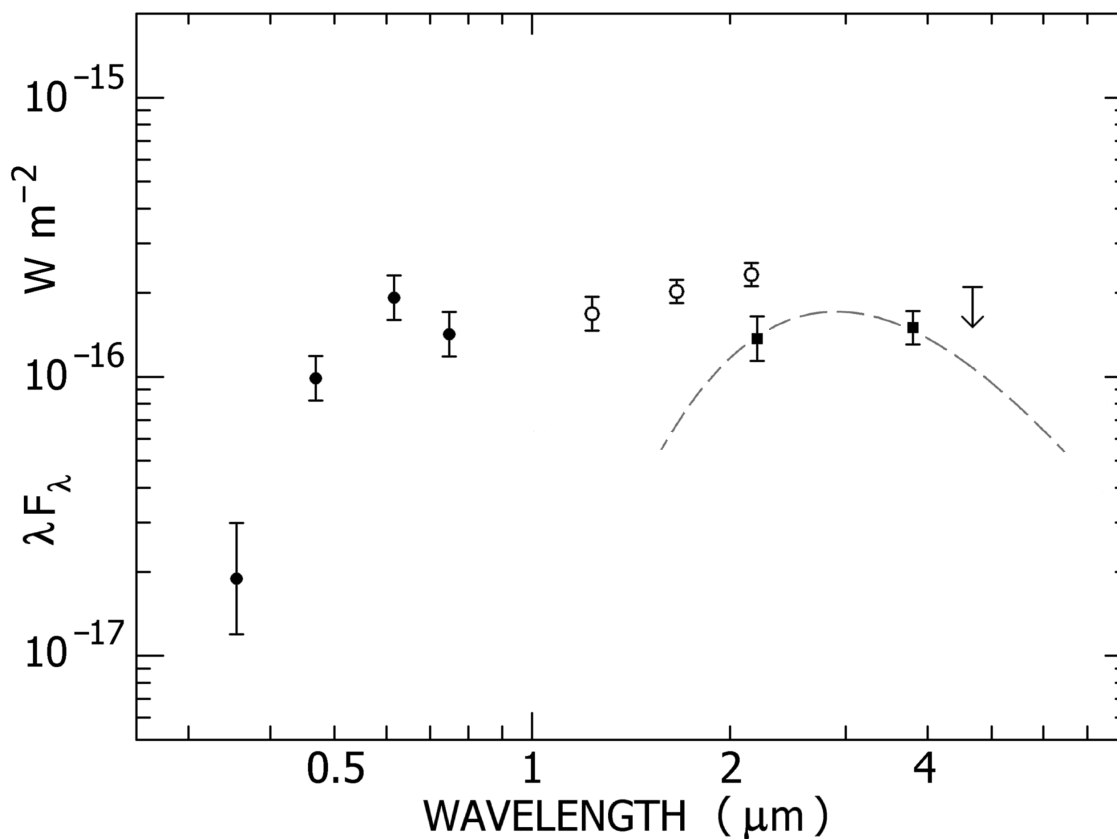


Fig. 2.— The post-plateau spectral energy distribution. The JHK_s photometry from 13 March 2012 is shown as open circles, the *ugri* magnitudes from 25 March 2012 as filled circles, and the $KL'M'$ photometry from 03 May 2012 as filled squares. Even though there is a gap of 7 weeks between the the two K-band measurements and SN2011ht had faded, the L' flux and M' upper limit confirm that SN2011ht formed dust during its rapid decline. The dashed curve shows the SED produced by dust at 900–1000 K, depending on the detailed emissivity function.

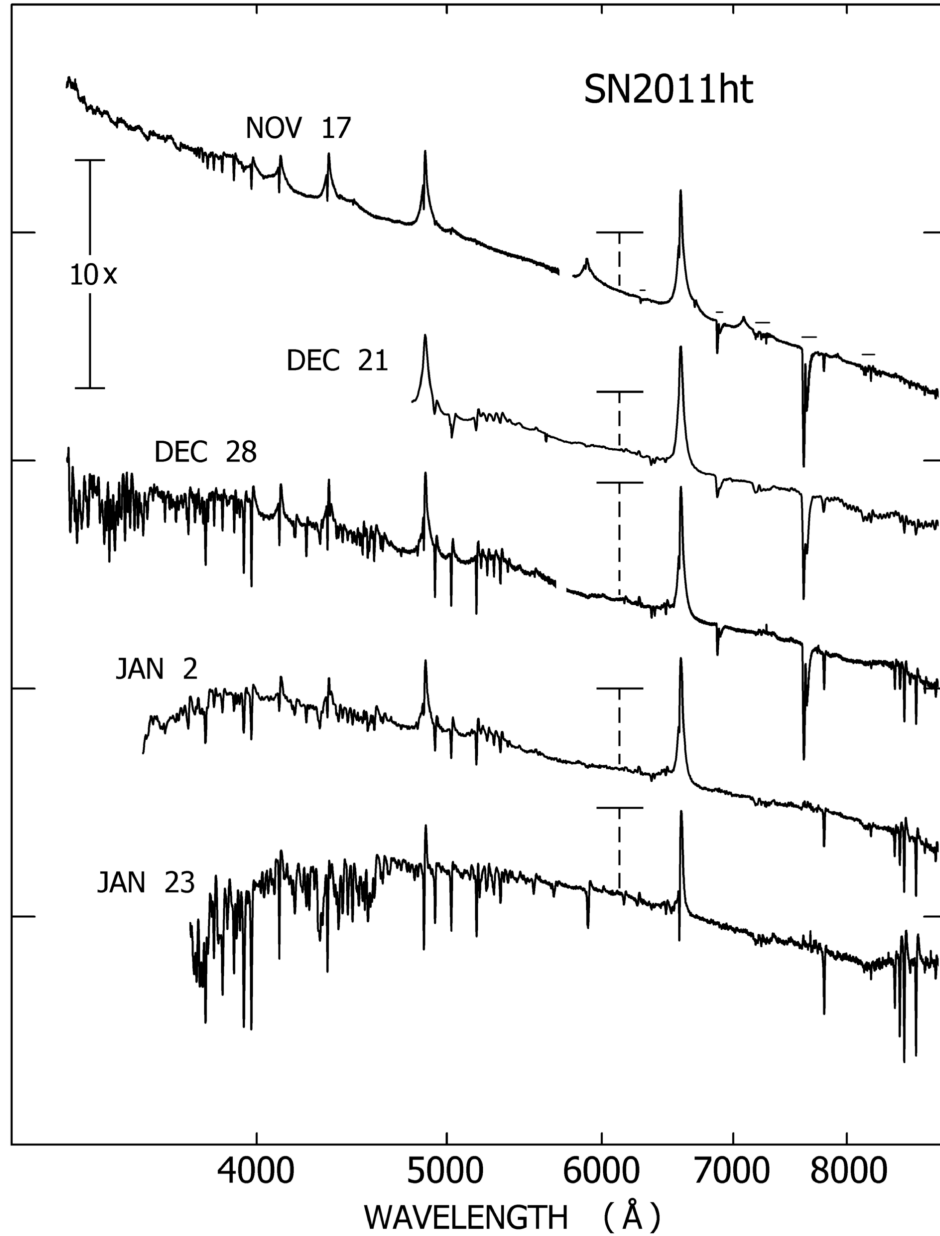


Fig. 3.— The spectra of SN2011ht from 17 November 2011 to 23 January 2012 showing the transition from the hot wind to the cool dense wind. See Table 3 for the details of each spectrum. The vertical scale is $\log F_\lambda$ and the bar above each spectrum marks the 10^{-14} ergs $\text{cm}^{-2} \text{s}^{-1} \text{\AA}^{-1}$ flux level. The last spectra from February 2012 are not included here because the flux had declined far below the level on 23 January, see Figure 7. The positions of the telluric bands due to O_2 and H_2O are marked with a short bar.

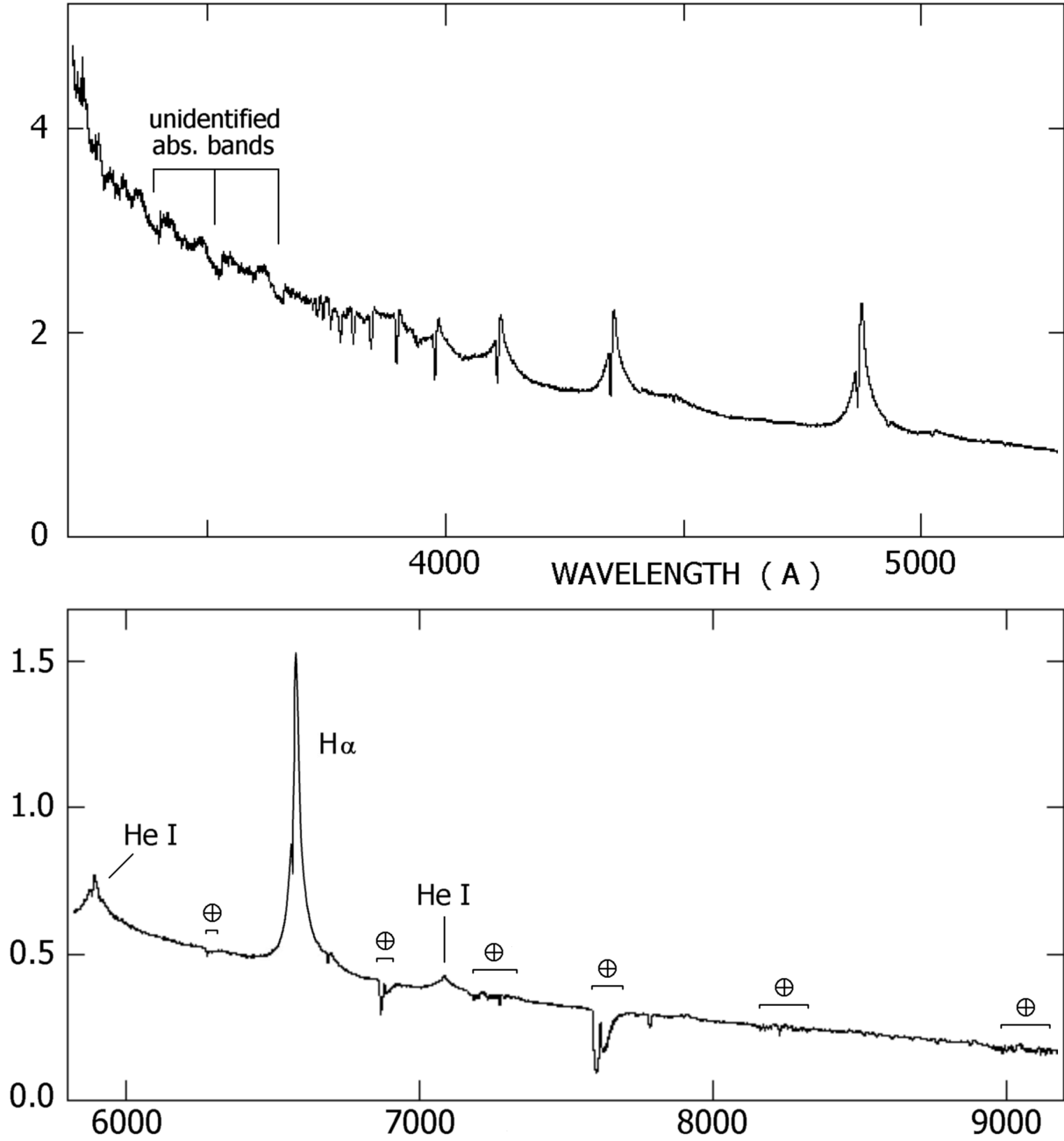


Fig. 4.— The blue (upper) and red (lower) MODS1 spectra from 17 November 2012 during the dense, hot wind stage. The vertical flux scale is in units of 10^{-14} ergs cm^{-2} s^{-1} \AA^{-1} . The very broad Thomson scattering wings in the Balmer lines and in He I $\lambda 7065$ and $\lambda 5876$ are obvious. The unidentified bands in the near-UV are marked, and the telluric bands are marked with \oplus .

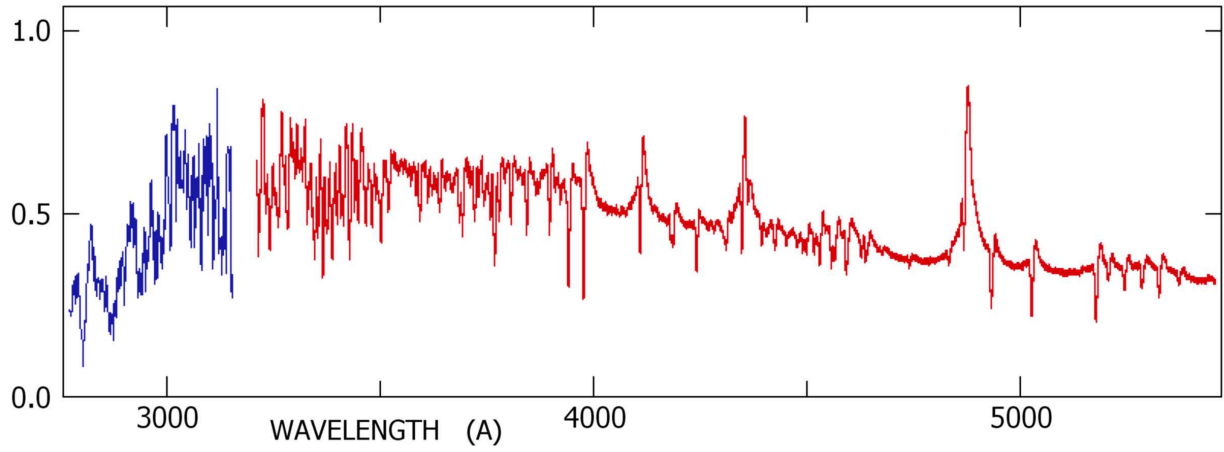


Fig. 5.— The MODS1 spectrum from 26 December 2011 with the nearly overlapping red side of the STIS/MAMA NUV2376 spectrum obtained the same day. The vertical flux scale is in units of 10^{-14} ergs cm^{-2} s^{-1} \AA^{-1} . Note the appearance of deep Fe II and Ca II H and K absorption lines.

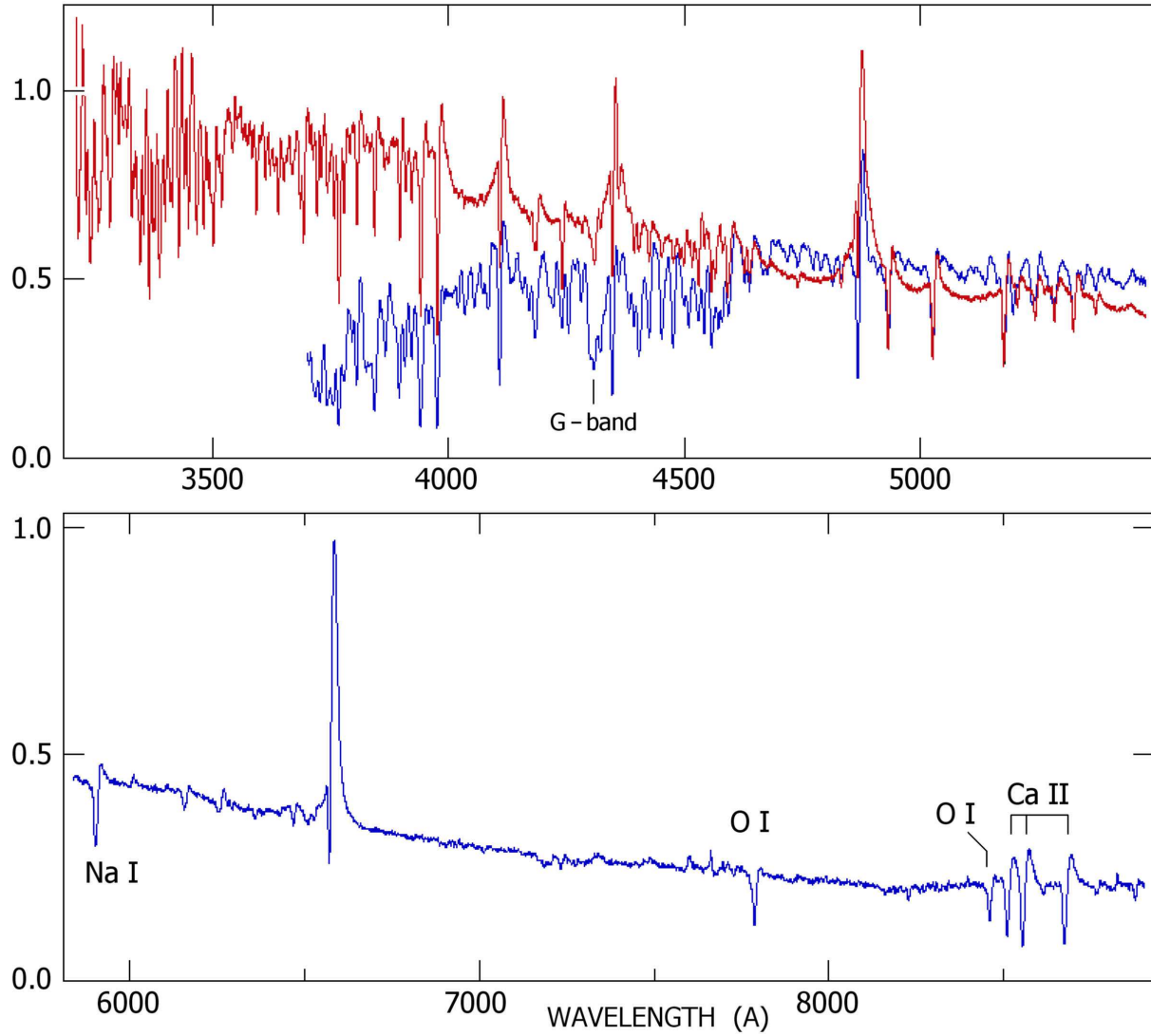


Fig. 6.— Upper: The MODS1 26 December 2011 blue spectrum with the MMT/Hectospec spectrum from 23 January 2012 illustrating the development of the cool dense wind. Lower: The MMT/Hectospec red spectrum from 23 January 2012. The Ca II triplet shows well developed P Cygni profiles. The vertical flux scale is in units of 10^{-14} ergs cm^{-2} s^{-1} \AA^{-1} .

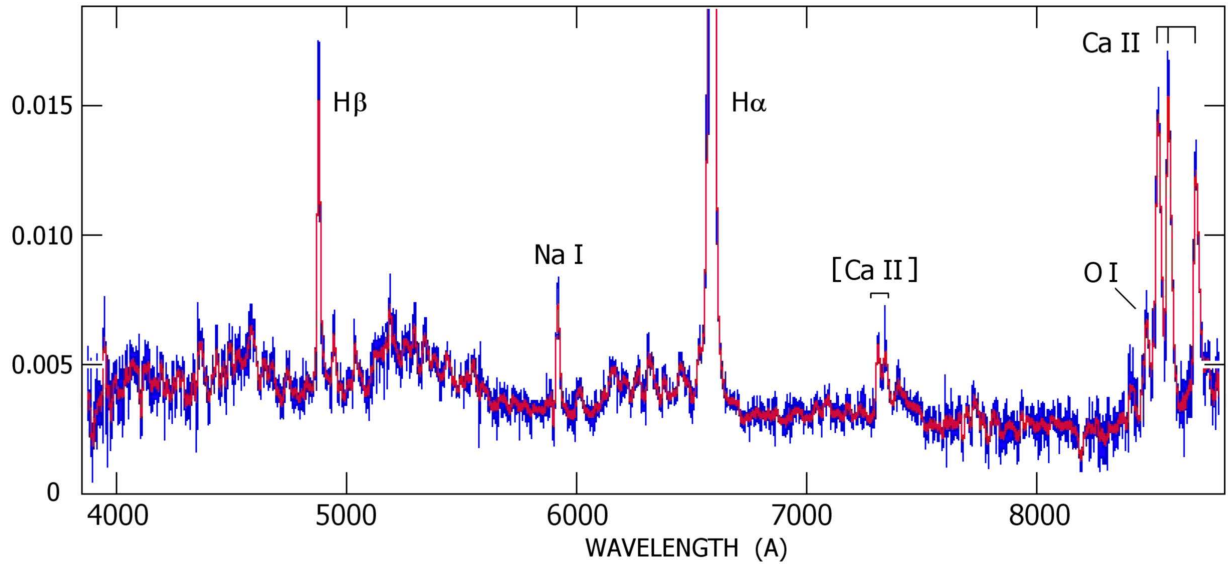


Fig. 7.— Two post-plateau spectra obtained during the photometric decline from 13 February 2012 with the MMT/Hectospec in blue and from 28 February with the ARC DIS in red. The vertical flux scale is in units of 10^{-14} ergs cm^{-2} s^{-1} Å^{-1} .

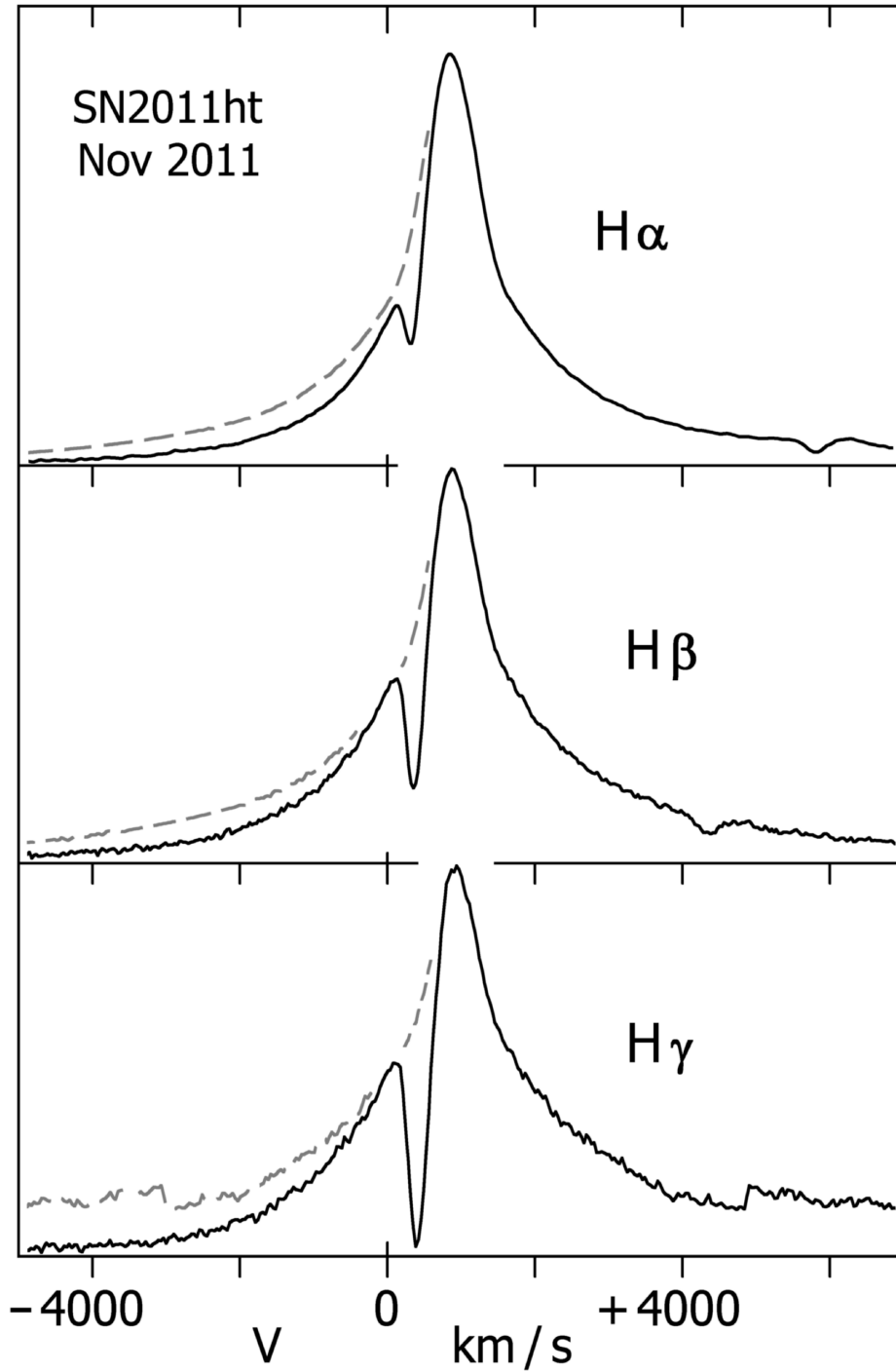


Fig. 8.— The H α , H β and H γ emission profiles from the 17 November 2011 MODS1 spectrum. To illustrate the asymmetry we mirror the red wing as a dashed curve on the left side of each profile; compare with Figure 11 in Dessart et al. Weak He I emission on the red side of H α and H β is clearly too weak to alter the basic profile. Heliocentric velocities are shown.